Published online 10 April 2013 *Nucleic Acids Research, 2013, Vol. 41, No. 10* ***5235–5250***
doi:10.1093/nar/gkt217

Quantitative *in vivo* analysis of chromatin binding of Polycomb and Trithorax group proteins reveals retention of ASH1 on mitotic chromatin

Philipp A. Steffen[1], João Pedro Fonseca[1], Cornelia Gänger[1], Eva Dworschak[1], Tobias Kockmann[2], Christian Beisel[2] and Leonie Ringrose[1,*]

[1]Institute of Molecular Biotechnology (IMBA), Dr. Bohr-Gasse 3, 1030 Vienna, Austria and [2]Department of Biosystems Science and Engineering, ETH Zürich, Mattenstrasse 26, 4058 Basel, Switzerland

Received November 8, 2012; Revised February 15, 2013; Accepted March 8, 2013

ABSTRACT

The Polycomb (PcG) and Trithorax (TrxG) group proteins work antagonistically on several hundred developmentally important target genes, giving stable mitotic memory, but also allowing flexibility of gene expression states. How this is achieved in quantitative terms is poorly understood. Here, we present a quantitative kinetic analysis in living *Drosophila* of the PcG proteins Enhancer of Zeste, (E(Z)), Pleiohomeotic (PHO) and Polycomb (PC) and the TrxG protein absent, small or homeotic discs 1 (ASH1). Fluorescence recovery after photobleaching and fluorescence correlation spectroscopy reveal highly dynamic chromatin binding behaviour for all proteins, with exchange occurring within seconds. We show that although the PcG proteins substantially dissociate from mitotic chromatin, ASH1 remains robustly associated with chromatin throughout mitosis. Finally, we show that chromatin binding by ASH1 and PC switches from an antagonistic relationship in interphase, to a cooperative one during mitosis. These results provide quantitative insights into PcG and TrxG chromatin-binding dynamics and have implications for our understanding of the molecular nature of epigenetic memory.

INTRODUCTION

The highly conserved Polycomb (PcG) and Trithorax (TrxG) group proteins constitute a gene regulatory system that is essential for maintaining the correct identity of both stem cells and differentiated cells (1,2). The PcG and TrxG proteins share several hundred developmentally important target genes (3–5). These two groups of proteins work antagonistically to maintain a balance between silencing (PcG) and activation (TrxG) of their targets (6). For several target genes, reporter assays have shown that the PcG and TrxG can maintain mitotically heritable stable states of both silent (7,8) and activated gene expression (9–11) depending on the initial transcriptional status of the target gene. Thus, these proteins have the capacity to maintain stable epigenetic memory of transcriptional decisions, in the absence of the initial determining transcription factors. However, this regulatory system also has an inherent flexibility, allowing PcG and TrxG target genes to switch their transcriptional status dynamically on developmental or experimental cues (9,12). The PcG and TrxG proteins function in several large multiprotein complexes, and in *Drosophila,* are recruited to their targets via multiple sequence-specific DNA-binding proteins (13,14). Thus, many chromatin-binding components work together, giving a dynamic balance between stable mitotic propagation of transcriptional states and flexibility of these states to allow developmental transitions.

Live imaging studies have given important insights into the dynamic nature of chromatin binding for some components of this system (15–17). The Polycomb repressive complex 1 (PRC1) contains several proteins, including Polycomb (PC) and Polyhomeotic (PH). In flies, both of these proteins have been shown to bind dynamically to chromatin, with exchange of bound molecules occurring within seconds (17). These studies demonstrate that PRC1 complexes bind chromatin by simple chemical equilibria (15). Given this observation, it has been proposed that developmental transitions in PcG and TrxG regulation may be a matter of quantitative, rather than qualitative change (18). To understand dynamic aspects of regulation by PcG and TrxG proteins, it is crucial to gain quantitative information about their absolute molecule numbers, molar concentrations and kinetic chromatin-binding properties in living animals. We have recently reported a quantitative analysis of these parameters for the PRC1 proteins PC and PH in living *Drosophila* (17). However, for other components of the PcG/TrxG system, such as

*To whom correspondence should be addressed. Tel: +431 79044 4650; Fax: +431 79044 110; Email: Leonie.Ringrose@imba.oeaw.ac.at

PRC2 proteins, DNA-binding proteins and the TrxG proteins, whether they also bind dynamically to chromatin, and whether different proteins have different kinetics, is unknown. Furthermore, quantitative information on molecule numbers and cellular concentrations is lacking. This puts limits on modelling and systems biology approaches aiming at the understanding of Polycomb and Trithorax group proteins as a complex and dynamic system.

To understand PcG and TrxG function, quantitative knowledge of chromatin-binding dynamics is essential not only in interphase but also throughout the cell cycle, where the most important challenges for the propagation of epigenetic memory are at replication and mitosis. Recent studies have shown that some PcG and TrxG proteins can bind to newly replicated chromatin, providing models for propagation of information at the replication fork (19–23). However, the behaviour of these proteins during mitosis is less well studied. Live imaging and immunofluorescence studies have demonstrated substantial dissociation of PRC1 proteins during mitosis (17,24,25). Different immunofluorescence studies of the human TrxG protein MLL have reported dissociation from mitotic chromatin (26) or robust association (27). We have recently shown by quantitative live imaging that a small fraction of *Drosophila* PC molecules remains bound to mitotic chromatin in both neuroblasts (NBs) and sensory organ precursor cells (SOPs) (17). Remarkably, this subpopulation of molecules binds mitotic chromatin with up to 300-fold longer residence times than in interphase, indicating that the nature of the PC–chromatin interaction is profoundly altered at mitosis. Importantly, the extent and strength of PC binding to mitotic chromatin is highly cell-type specific, suggesting that regulation of this mitotic association may be important for epigenetic memory and cell identity. A comprehensive understanding of the regulation of mitotic chromatin association requires quantitative analysis of more components of the PcG and TrxG system, in terms of whether and how they bind mitotic chromatin in living animals, and how they interact with each other.

Here, we present a quantitative live imaging analysis of the *Drosophila* PRC2 protein enhancer of Zeste (E(Z)), the DNA-binding protein Pleiohomeotic (PHO) and the TrxG protein absent, small or homeotic discs 1 (ASH1). These proteins represent several different functions within the PcG/TrxG regulatory system; thus, we envisaged that they may have specific kinetic properties related to their functions. We quantify absolute molecule numbers, cellular concentrations and kinetic chromatin-binding properties of all three proteins in living animals, and we compare them with those of PC. We show that all of the proteins bind remarkably dynamically to interphase chromatin, exchanging like PC, within seconds. We quantify different extents of mitotic dissociation for each protein, with ASH1 showing the most robust and abundant association with metaphase chromatin in several cell types. Finally, we present the surprising finding that although ASH1 limits the residence time of PC on interphase chromatin, it is required for the long residence time of PC in metaphase, indicating a switch from an antagonistic to a cooperative relationship between these two proteins during mitosis. In summary, this study constitutes a quantitative kinetic analysis of key components of an epigenetic system, providing several unexpected insights into their dynamics and interdependence of chromatin binding and the potential molecular nature of mitotic memory.

MATERIALS AND METHODS

Transgenic fly lines expressing EGFP fusion proteins

Generation of PcG/TrxG enhanced green fluorescent protein (EGFP) fusion protein fly lines is described in detail in Supplementary Methods. Constructs, sequences, plasmid maps and fly lines are available on request. For details of fly strains and crosses and *ash1* knockdown experiments, see Supplementary Methods.

Quantification of protein expression levels and molecule numbers

Quantification of PC, PHO and ASH1 was performed on nuclear extracts, and quantification of E(Z) expression levels was performed on whole-cell extracts, as described in Supplementary Materials and Methods. Ratios were calculated as described in the legend of Figure 1. Calculation of molecule numbers via virus-like particle (VLP) calibration of EGFP was performed as described previously (17) and as given in the legend of Supplementary Table S1. Calculation of molecule numbers via fluorescence correlation spectroscopy (FCS)-based calibration of EGFP is described under FCS later in the text.

Live imaging

Live imaging of SOP and NB lineages was performed as described previously (17), see also Supplementary Methods. For embryo live imaging, embryos were collected on apple juice–agar plates for 60 min and dechorionated using a 50% solution of household bleach (2.8% hypochlorite) for 2 min. Embryos were lined up on a filter and transferred onto a No. 1.5 coverslip (Menzel) coated with embryo glue (28) and covered with Voltalef 10S oil. Live imaging of PcG/TrxG proteins during embryogenesis was performed at room temperature on a Zeiss Confocal Laser Scanning Microscope LSM780 with a 40×/NA 1.3 oil immersion objective. Z-stacks were recorded every 15 s to generate a time-lapse movie of early nuclear divisions. Image planes of 512 × 512 px were acquired with a zoom of 4.3 resulting in a voxelsize of 100 × 100 × 800 nm. EGFP was excited with an Argon laser at 488 nm [acousto-optical tunable filter (AOTF): PC: 0.5%, E(Z): 1%, ASH1: 2%, PHO: 3%] and detected between 490–578 nm (Gain: PC, E(Z): 650V, ASH1: 700V, PHO: 750V). The pinhole was set to 90 µm. Images were deconvolved using Huygens Core (SVI) with the Classic Maximum Likelihood Estimation (CLME) method and 40 iterations and a theoretical point spread function (PSF). Maximum intensity projections were calculated from the deconvolved z-stacks. To analyse mitotic chromatin attachment, average line

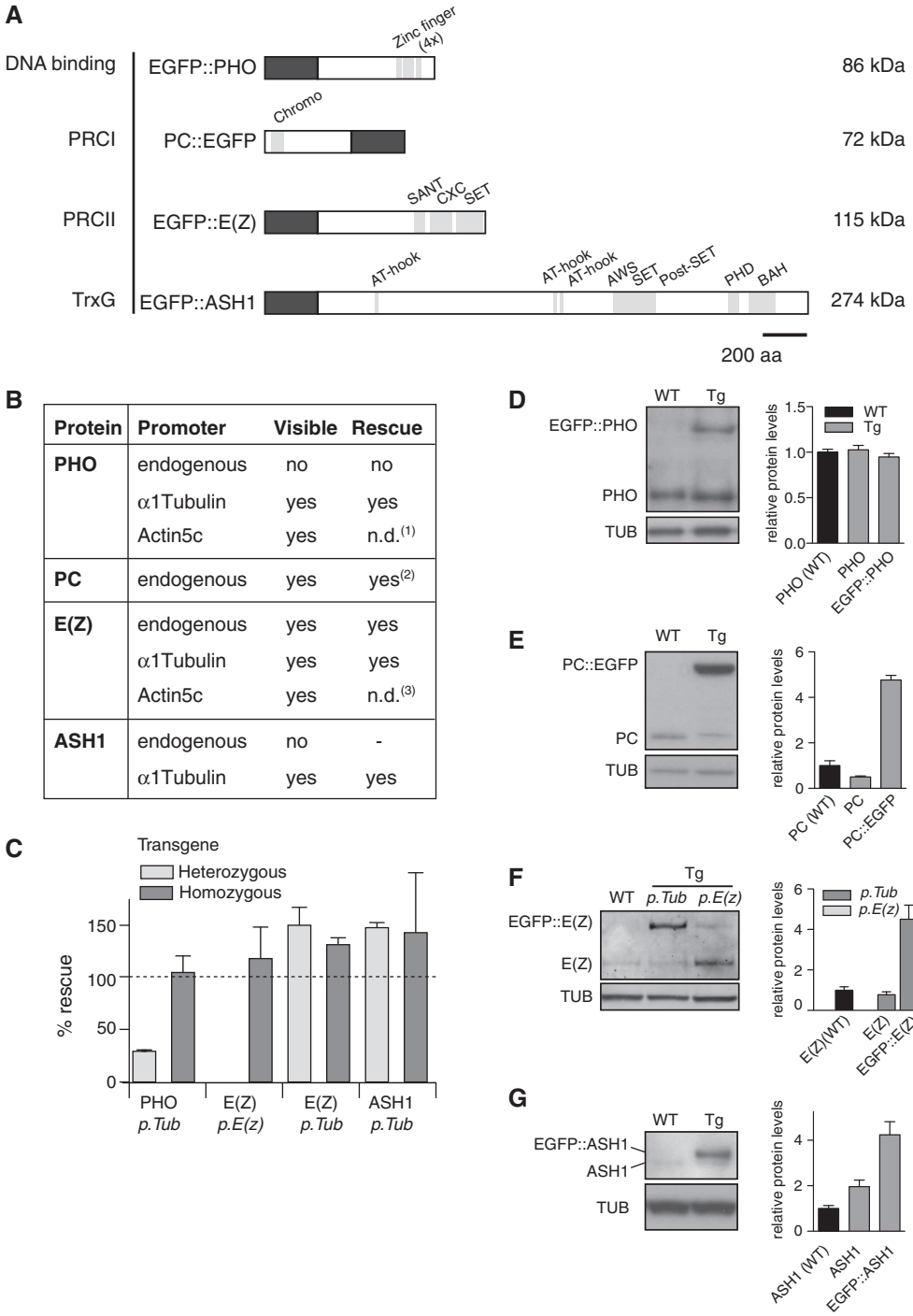

Figure 1. Generation of transgenic EGFP-tagged PcG/TrxG fly lines. (**A**) Schematic representation of EGFP fusion proteins. Shown are domains according to UNIPROT (light grey), the position of the EGFP tag (dark grey) and the size of the fusion protein in kDa. Proteins are drawn to scale. EGFP::PHO, EGFP::E(Z), EGFP::ASH1, this study; PC::EGFP (25). (**B**) Transgenes were generated with different promoters as shown. All of the lines shown gave viable homozygous stocks. The table shows whether the fusion protein was visible by fluorescence microscopy in larval salivary glands and embryos, and whether it was able to rescue lethal combinations of mutant alleles as follows: EGFP::PHO expressed under the *αTubulin* promoter rescued pho^1/pho^1. (1) flies carrying *Actin5c* driven EGFP::PHO with appropriate balancers (Supplementary Figure S1) could not be generated, see 'Materials and Methods' section. (2) PC::EGFP rescued Pc^3/Pc^{XL5} but not Pc^3/Pc^3 (17,25). EGFP::E(Z) driven by the endogenous or *αTubulin* promoters rescued $E(z)^{731}/E(z)^{63E11}$. (3) Rescue was not performed with *Actin5c* driven EGFP::E(Z), as the *αTubulin* promoter gave full rescue. EGFP::ASH1 driven by the *αTubulin* promoter rescued three combinations of alleles: $ash1^{10}/ash1^{22}$, $ash1^{22}/(3L)Exel9011$ and $ash1^{10}/Df(3L)Exel9011$. (**C**) For selected lines, percentage of rescue is calculated for heterozygous (light grey) or homozygous (dark grey) transgenes (Supplementary Figure S1 and 'Materials and Methods' section). EGFP::ASH1 rescue is shown for $ash1^{22}/(3L)Exel9011$. Mean and standard deviations of two independent experiments are shown. Numbers of scored flies: 1115 (PHO), 1346 (E(Z) *p.Tub*), 1115 (E(Z) *p.E(z)*, 235 (ASH1) (ASH1 rescues performed with other allele combinations see Supplementary Figure S1). (**D–G**) Left: western blot using antibodies against endogenous proteins. Extracts were prepared from 2- to 3-h-old embryo collections. PHO, PC and ASH1: nuclear extracts, E(Z): whole cell extract. 'WT' the parental landing site line. 'Tg' homozygous transgenic line. Right: quantification of expression levels. Black: (WT): endogenous protein in WT line is set to 1. Grey: levels of the endogenous and EGFP fusion protein in the transgenic line are shown relative to the endogenous protein in WT. Mean and standard error from at least three independent extracts are shown.

profiles were generated by measuring lines (140 px) perpendicular to the mitotic chromatin in nine nuclei per image.

Fluorescence recovery after photobleaching

Fluorescence recovery after photobleaching (FRAP) in SOP and type I NB lineages was performed as described previously (17). In embryos, FRAP experiments were performed similarly to our previous study (17) with the following modifications: FRAP was performed on a Zeiss LSM710 using 40×/NA 1.3 lens and a pinhole of 100 µm. Zoom factor 10 results in images with a pixelsize of 42 nm. Images (512 × 75 px) were acquired every 16–25 ms. EGFP was excited with an Argon laser at 488 nm (AOTF: 0.5–1%) and detected between 490–600 nm (Gain: 500–700V). In general, laser intensities were kept as low as possible to minimize unintentional photobleaching. A circular region with a radius of 15 px in the centre of the image was bleached using 2 bleach pulses with 100% of the 488 nm Argon laser. Intensity measurements of the bleached region and a control region for background correction, as well as a control image series without bleach for normalization of unintentional photobleaching, were performed using an in-house developed MATLAB script, which uses the function tiffread.m (29) (code available on request). A reaction–diffusion model (30) was used to extract kinetic parameters from FRAP recovery curves as described in detail previously (17).

Fluorescence correlation spectroscopy

FCS experiments were performed on a Zeiss LSM780 microscope using a 40×/NA 1.3 lens. EGFP was excited using the 488 nm line of an Argon laser with the AOTF set to 0.2% and a pinhole of 1 airy unit. Autocorrelation curves (ACFs) were acquired using the microscope software ZEN from intensity fluctuations measured for 5 s. Multiple measurements per nucleus were averaged to generate an ACF that was then used to extract kinetic parameters in MATLAB using a reaction–diffusion model (31). The FCS measurement volume ($V = 0.104 \pm 0.042\,\mu m^3$) was calibrated using FCS measurements of a fluorescein concentration series by measuring concentrations between 5 and 100 nM and determining n from the ACF using $Df = 425\,\mu m^2/s$ (32). Extrapolation of molecule numbers in the whole nucleus was done by multiplication of n determined from the ACF with the ratio $V_{nucleus}/V_{FCS} = 2145$. The average volume of a nucleus during cycle 12 of embryogenesis ($V_{nucleus}$) was determined by measuring volumes of five nuclei in a 3D reconstruction of H2B::red fluorescent protein (RFP)-marked chromatin ($V_{nucleus} = 222.6 \pm 7.5\,\mu m^3$).

RESULTS

EGFP fusions of Polycomb and Trithorax group proteins: tools for live imaging

The PRC1 proteins PC and PH have been shown to bind dynamically to chromatin in embryos (15) and in larval and pupal cells (15,17). To investigate kinetic properties of other PcG and TrxG proteins, we generated transgenic flies carrying EGFP fusions of selected proteins (Figure 1A). We chose the DNA-binding protein PHO, the PRC2 protein E(Z) and the Trithorax group protein ASH1. The PHO protein recruits other PcG proteins to DNA via its sequence-specific DNA-binding activity (33–36). The E(Z) protein is a histone methyltransferase that methylates histone H3 on lysine 27, creating a binding platform for PRC1 (37). ASH1 is a histone methyltransferase that methylates Histone H3 on lysine 36 (38). This modification has been shown to antagonize PRC2-mediated H3K27 methylation (39). ChIP profiling shows co-localization of these proteins with PRC1 proteins at many target sites (3–5). In summary, the selected proteins not only interact with DNA and/or chromatin via different platforms but also interact with each other by distinct mechanisms. Thus, we reasoned that a comparison of their dynamic chromatin-binding properties may be highly informative.

To screen for optimal expression levels for both viability and live imaging, each EGFP fusion was cloned downstream of three different promoters, namely, *Actin5C*, *αTubulin* and the presumed endogenous promoter, defined as the region upstream of the gene of interest, extending to the next adjacent annotated gene region (see 'Materials and Methods' section). For comparison, the published PC::EGFP transgene, under control of the endogenous PC promoter, was included in the analysis [Figure 1A; (25)]. EGFP::PHO, EGFP::EZ and EGFP::ASH1 transgenes were inserted at the same landing site using ΦC31-mediated site-specific integration (40).

Transgenes were recovered from all injected constructs (Figure 1B). To ascertain their usefulness for live imaging, all transgenic lines were evaluated for their EGFP expression levels in larval salivary glands and embryos, showing that with the exception of EGFP::ASH1 and EGFP::PHO under control of the presumed endogenous promoters, all lines gave a visible EGFP signal (Figure 1B). To determine whether these PHO, E(Z) and ASH1 fusion proteins are functional, as well as visible, each was tested for its ability to rescue lethal combinations of alleles of the respective gene (Figure 1B and C, Supplementary Figure S1 and 'Materials and Methods' section). Each of the three fusions was able to rescue lethality, with the extent of rescue depending on the expression strategy used (Figure 1C). The apparent rescue to >100% for E(Z) and ASH1 under the *αTubulin* promoter arises from underrepresentation of other genotypes in the progeny of the rescue cross (Supplementary Figure S1). This analysis demonstrates that all three of the novel fusion proteins are able to fulfil the functions of their endogenous counterparts.

To determine the expression levels of the fusion proteins in relation to those of the endogenous proteins, we performed quantitative western blots on embryos (Figure 1D–G and Supplementary Figure S2) and in third instar larval brains (Supplementary Figure S3). Quantification of signals revealed that the fusion proteins were expressed at between 0.3- and 4.8-fold compared with the endogenous protein. Each protein

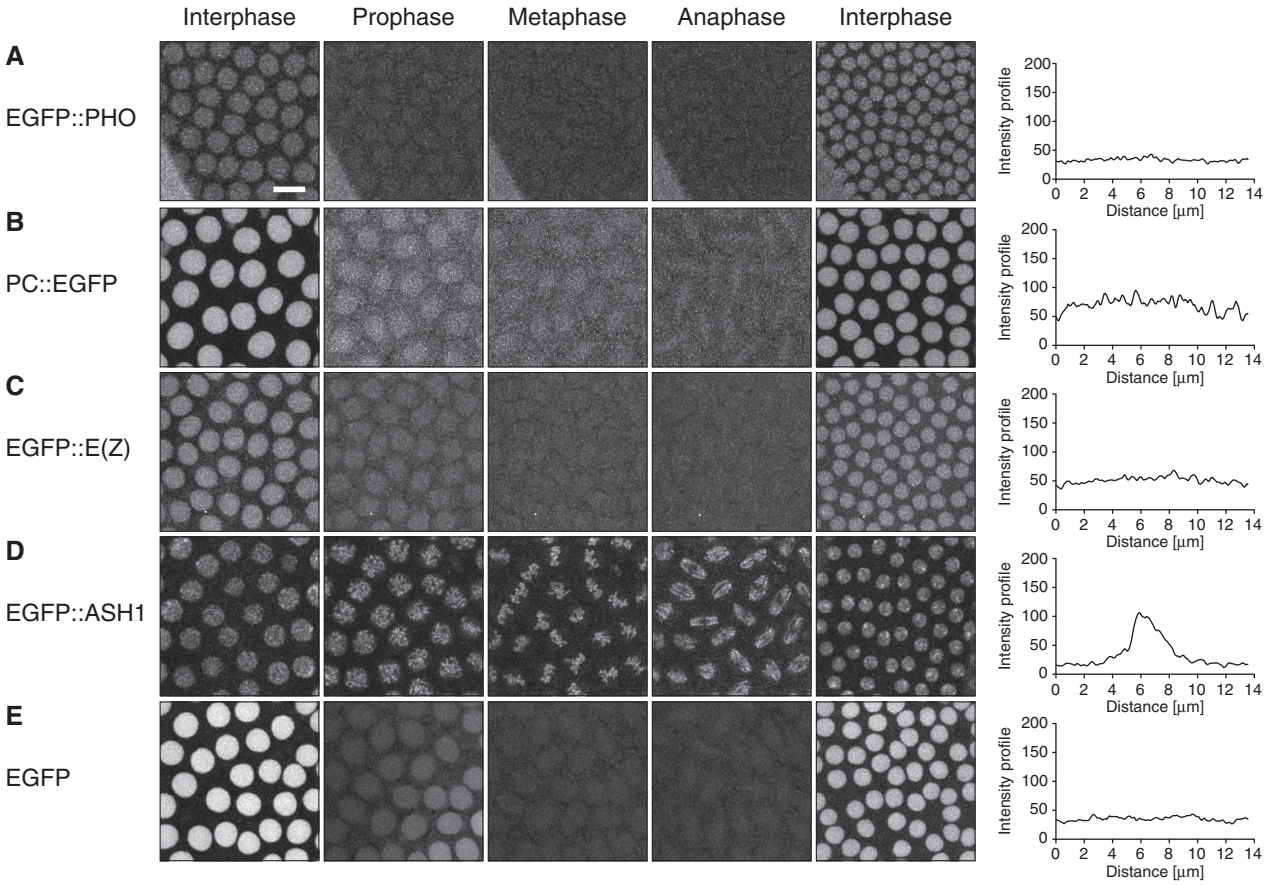

Figure 2. Time-lapse microscopy of PcG/TrxG EGFP fusion proteins during blastoderm embryogenesis. Left: Living blastoderm embryos were imaged using confocal microscopy to visualize expression and localization of PcG/TrxG fusion proteins (**A–D**) and EGFPnls (**E**) during cleavage cycles 10–13 of embryogenesis. Shown are individual timepoints corresponding to different cell cycle phases, as indicated. Images are maximum-intensity projections of z-stacks from deconvolved time-lapse experiments. Scale bar represents 10 µm and is the same for all images. Right: averaged line profiles through nine individual nuclei within the maximum-intensity projections at metaphase shown in images (left) were measured. The line was chosen to be perpendicular to the mitotic chromatin plate. The *y*-axis shows the raw average intensity along the lines.

was expressed at similar levels in embryos (Figure 1D–G) and in larval brains (Supplementary Figure S3), and levels were relatively stable throughout embryonic development (Supplementary Figure S2). Interestingly, the presence of the E(Z) transgene under its own promoter led to substantial upregulation of the endogenous E(Z) protein (Figure 1F). Cross-regulation between PC::EGFP and PH::EGFP transgenes has been observed previously, where the presence of the transgene led to downregulation of the endogenous copy [(15,17), this effect is also visible in Figure 1E]. In summary, we have generated three novel transgenic PcG and TrxG fusion proteins that have ideal properties as tools for live imaging: they are expressed at moderate levels in transgenic animals, but nevertheless give sufficient signal for imaging in living tissues.

The TrxG protein ASH1 binds mitotic chromatin in embryos

Early *Drosophila* embryogenesis provides an ideal system to study mitosis. The nuclei of the syncytial embryo divide 13 times synchronously before cellularization (blastoderm). Divisions occur rapidly within 9–21 min (41) and are characterized by an altered cell cycle with severely shortened G_1/G_2 phases. Zygotic transcription starts just before blastoderm, and proteins observed before this stage are, therefore, maternally contributed, either as proteins or mRNAs.

To investigate the behaviour of PHO, E(Z) and ASH1 during the cell cycle, and to compare it with that of PC, we performed time-lapse confocal microscopy of preblastoderm mitotic divisions in living transgenic embryos. The *αTubulin* driven constructs are used in this and all subsequent experiments unless otherwise stated. This analysis revealed characteristic behaviour of each EGFP::fusion protein. EGFP::PHO was undetectable by the onset of prophase, and it did not reappear until the next interphase (Figure 2A), suggesting complete dissociation from mitotic chromatin in early embryos. However, we note that EGFP::PHO showed the lowest EGFP levels of all fusion proteins; thus, we cannot exclude that mitotic binding is present but undetectable. PC::EGFP was detectable in the vicinity of chromatin throughout mitosis, but did not show specific localization to mitotic chromosomes (compare Figures 2B and D). This is consistent with previous observations of mitotic behaviour of PC in embryos (24,25). EGFP::E(Z) was essentially undetectable

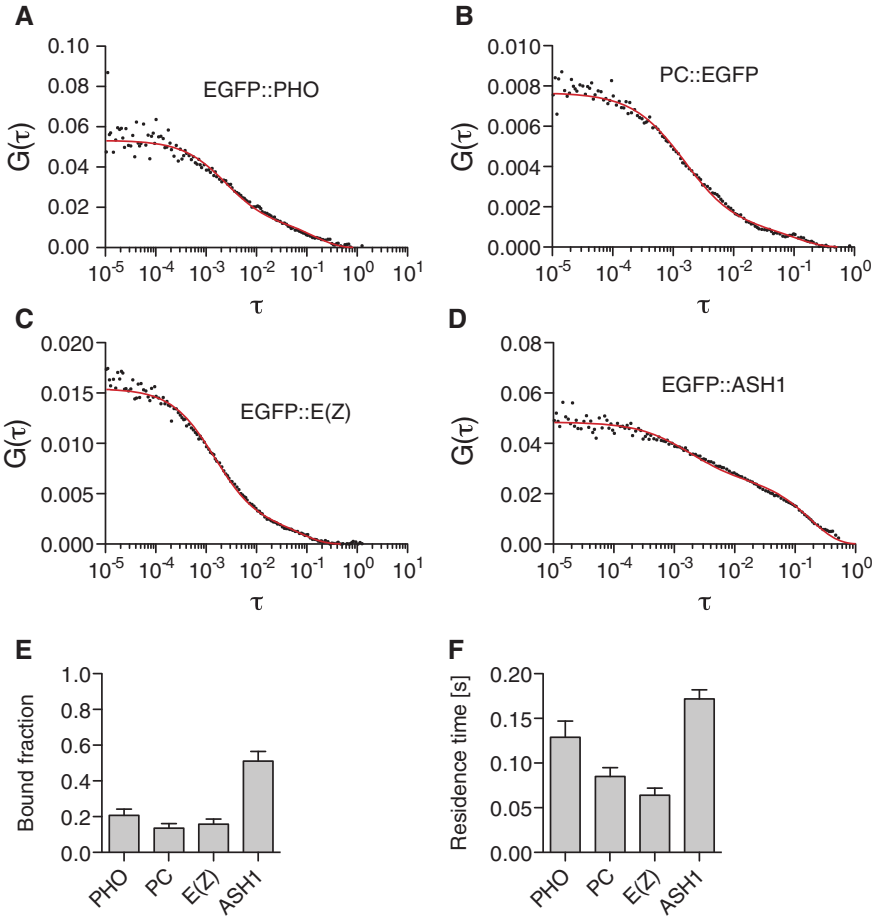

Figure 3. *In vivo* kinetics of chromatin binding of PcG and TrxG proteins measured by FCS in embryos. FCS was performed in preblastoderm embryos, at cleavage cycles 10–13. (**A–D**) Auto-correlation curves of EGFP::PHO, PC::EGFP, EGFP::E(Z) and EGFP::ASH1. G(τ): auto-correlation; τ: correlation time [s]. All transgenes except PC::EGFP are under *αTubulin* promoter control. (**E**) Bound fractions were calculated from mean values of k^*_{on} and k_{off} shown in Supplementary Figure S6 and Supplementary Table S1, as $k^*_{on}/(k^*_{on}+k_{off})$. (**F**) Residence times were calculated as $1/k_{off}$. Mean and cumulative standard errors of at least nine nuclei in at least two different embryos are shown.

during metaphase and anaphase, suggesting complete dissociation (Figure 2C). Metaphase lasts for 3–5 min, suggesting that degradation and re-synthesis of proteins is unlikely to explain the observed protein re-localization after mitosis. Consistent with this, quantification of EGFP intensities for all fusion proteins in other cell types revealed little or no reduction in protein levels during mitosis (Supplementary Table S1, row B), again arguing against mitotic degradation of specific proteins. Thus, we reason that the dissociation of PcG proteins from chromatin during prophase would lead to the redistribution of the protein throughout the syncytial embryo. In contrast, EGFP::ASH1 showed robust association with chromatin throughout the entire mitotic cycle (Figure 2D). To determine whether mitotic association is a common feature of TrxG proteins, we performed immunofluorescence analysis of the TrxG proteins TRX and OSA, showing that TRX, but not OSA, was detectable on mitotic chromatin (Supplementary Figure S4).

In summary, this analysis shows that although the PcG proteins substantially dissociate from chromatin and re-associate at different times during the mitotic cycle, the TrxG proteins ASH1 and TRX remain associated with chromatin throughout mitosis.

Quantitative kinetic analysis reveals highly dynamic chromatin-binding behaviour for all proteins

To determine whether PHO, EZ and ASH1 EGFP fusion proteins show dynamic chromatin binding, we performed quantitative kinetic analysis on preblastoderm embryos and compared the binding kinetics of these three proteins with those of PC::EGFP. We have previously measured interphase kinetics of the same PC::EGFP fusion protein in NBs and SOPs, showing residence times of a few seconds (17). To obtain several independent measures of binding kinetics, we performed and compared both FRAP (Supplementary Figure S5) and FCS (Figure 3 and Supplementary Figures S6 and S7). FCS was performed for all four fusion proteins, whereas the low expression level of EGFP::PHO precluded the use of FRAP for this protein. To enable comparisons between the two techniques, both FRAP and FCS data were analysed using reaction–diffusion models that have recently been developed for each technique [FRAP: (30), FCS: (31)].

These models enable extraction of values for the diffusion coefficient, (*Df*) the pseudo first order association rate (k^*_{on}) and the dissociation rate (k_{off}). Comparison of different fitting procedures showed contributions of binding to the kinetics of all four proteins (data not shown), and FRAP data showed a contribution of diffusion to the recovery kinetics of the three proteins thus studied (Supplementary Figure S8). Thus, the full model with all three parameters was used for analysis of all data, enabling comparisons both between the techniques and between the different proteins. A full list of kinetic parameters for each protein is given in Supplementary Table S1.

To control for the effects of fusion protein overexpression on kinetic behaviour, we used two strategies. First, we compared the kinetics of EGFP::E(Z) under the control of the *αTubulin* and *Actin5C* promoters, which gave different levels of EGFP::E(Z) protein. Analysis of parameters extracted from both FRAP and FCS data revealed no significant differences in the values of k^*_{on} and k_{off}; thus, the expression level of EGFP::E(Z) does not detectably affect the inherent kinetic properties of the fusion protein [Supplementary Figures S5G–N and S6, compare E(Z) *p.Tub* and E(Z) *p.Actin*]. Second, we compared the kinetics of EGFP::ASH1 under control of the *αTubulin* promoter in flies wild-type for endogenous *ash1*, to the same transgenic protein in an *ash1* mutant background. Strikingly, the kinetic behaviour of the EGFP::ASH1 protein measured by FRAP was identical in these two genetic backgrounds (Supplementary Figure S5G–N, compare ASH1 and ASH1 rescue), indicating again that the overexpression of protein in the wild-type background has no detectable effect on its kinetic behaviour.

Analysis by FRAP and FCS revealed that all four proteins bind chromatin dynamically (Figure 3 and Supplementary Figure S5). The extracted diffusion coefficients given by FCS and FRAP were in reasonably good agreement with each other, with the exception of EGFP:ASH1, for which a slower diffusion coefficient was extracted from FRAP than from FCS data (Supplementary Figure S7A). This may comprise both the true diffusion and a binding component, or may also be due to chromatin movements during the longer measurement times used in ASH1 FRAP experiments (18,30). In all cases, diffusion was slower than expected for the monomeric protein, suggesting that these proteins participate in high-molecular weight complexes (Supplementary Figure S7B).

The rate constants k^*_{on} and k_{off} that gave the best fit to the experimental data were an order of magnitude larger for FCS data than for FRAP data (Supplementary Figure S7C and D), leading to ~10-fold longer calculated residence times ($1/k_{off}$) from FRAP analysis than from FCS (Supplementary Figure S7E). A similar discrepancy between FCS and FRAP has recently been reported and has been attributed to photobleaching of bound molecules within the FCS volume (42). In addition, exploration of parameter space for FRAP data using simulations in which the k^*_{on} and k_{off} values were varied showed that a range of values gave similar fits to the data (Supplementary Figure S5B, D and F). Thus, the values extracted from FCS and FRAP may be considered as giving upper and lower limits to the true values of k^*_{on} and k_{off}. Importantly, the relationship between k^*_{on} and k_{off} was stringently constrained (Supplementary Figure S5B, D and F) and was reproducible between the two techniques and between different proteins (Supplementary Figure S7C and D). This is best seen in the calculated bound fractions [$= k^*_{on}/(k^*_{on} + k_{off})$], which were identical for FCS and FRAP (Figure 3E and Supplementary Figure S7F).

This analysis showed the highest bound fraction for EGFP::ASH1 of ~50–60% compared with 14–21% for the other three proteins (Figure 3E and Supplementary Figure S7F). EGFP::ASH1 also showed the longest residence time with both techniques, at ~2-fold longer than PC::EGFP and EGFP::E(Z) (Figure 3F and Supplementary Figure S7E). We have previously measured the kinetics of PC::EGFP by FRAP, using identical fitting procedures to those used here, in larval NBs and pupal SOPs (17). Interestingly, the residence time measured here by FRAP in embryos (Supplementary Figure S5N) was essentially identical to that measured in SOPs previously (17) (embryos 1.27 s, SOPs 1.39 s), but longer than that measured in NBs (0.46 s).

In summary, this quantitative kinetic analysis demonstrates that all four proteins tested show substantial binding to chromatin in early embryos, and that this binding is highly dynamic, with exchange between bound and free proteins occurring within seconds.

Absolute quantification reveals similar numbers of chromatin-bound molecules for all proteins

The kinetic analysis described earlier in the text measures relative quantities. Conversion of relative values to absolute numbers gives insights into concentrations of endogenous proteins and numbers of chromatin-bound molecules (17,18). To gain an estimate of absolute numbers of endogenous molecules, we used EGFP calibration in combination with quantitative western blotting (Figures 1D–G and 4). To obtain independent measurements of EGFP numbers, we used two methods of EGFP calibration, namely, imaging of EGFP-containing VLPs (43) and direct measurement of molecule numbers by FCS (Figure 4A and Supplementary Figure S9). Measurements were performed in preblastoderm embryos at syncytial division cycles 10–13. The average calculated numbers of EGFP molecules per nucleus were in excellent agreement between the two techniques, giving only 1.02-, 1.49- and 1.42-fold difference (VLP/FCS) for EGFP::PC, EGFP::E(Z) and EGFP::ASH1, respectively (Figure 4A). Thus, both EGFP calibration methods provide a robust basis for further calculations. We note that calibration by FCS has the advantage that both kinetic analysis and quantification are performed in the same cell. A full list of quantitative measurements for each protein is given in Supplementary Table S1.

EGFP numbers were converted to endogenous molecule numbers in wild-type flies via quantitative western blots as described previously (17) (Figure 1D–G). As a control for

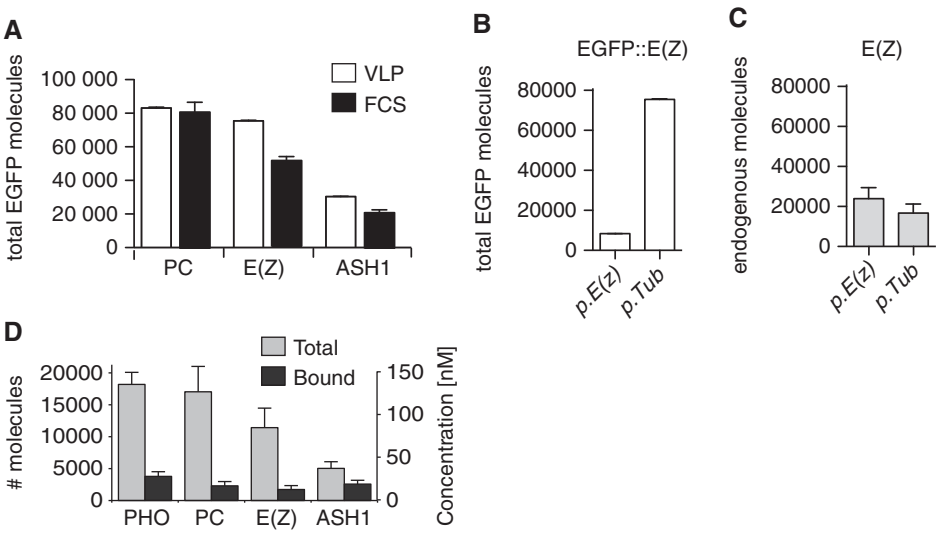

Figure 4. Quantification of endogenous molecule numbers of PcG and TrxG proteins in living embryos. (**A**) Estimated number per nucleus of EGFP molecules measured by EGFP–VLP calibration (white) or FCS (black) in preblastoderm embryos, at cleavage cycles 10–13. EGFP::E(Z) and EGFP::ASH1 were expressed from the *αTubulin* promoter. (**B**) Estimated number per nucleus of EGFP::E(Z) molecules, expressed from different promoters, measured by VLP calibration. EGFP::E(Z) was expressed from the endogenous *E(z)* promoter *(p.E(z))* or the *αTubulin* promoter *(p.Tub)*. (**C**) Estimated number per nucleus of endogenous E(Z) molecules in wild-type embryos, calculated from (**B**) via quantitative western blots (Figure 1F). Despite different EGFP expression levels from the two promoters, the calculated endogenous molecule numbers are similar. (**D**) Estimated total (light grey) and chromatin-bound (dark grey) molecule numbers (left axis) and nanomolar concentrations (right axis) per nucleus in preblastoderm embryos, at cleavage cycles 10–13, for four EGFP fusion proteins. Calculations were based on GFP calibration by FCS, and quantitative western blots are shown in Figure 1D–G. The volume used for calculation of concentrations (Supplementary Table S1) was the average nuclear volume at cycle 12 in interphase (between cleavage 11 and 12.). Data show the mean and cumulative standard error of at least nine nuclei.

the accuracy of western blot quantification, we compared the numbers of wild-type endogenous E(Z) molecules calculated using two different transgenes expressing EGFP::E(Z) at different levels (Figure 4B and C). Remarkably, despite a difference of ~10-fold in the EGFP numbers between the two transgenes (Figure 4B), the resulting calculated numbers of wild-type endogenous E(Z) molecules were highly similar, with only 1.42-fold difference [*p.E(z)*/*p.Tub*, Figure 4C]. This demonstrates that quantification by EGFP calibration and western blotting is robust over a wide range of signal intensities.

Further calculations taking into account the interphase nuclear volume and the chromatin-bound fractions measured by kinetic analysis in embryos enabled estimations of molar concentrations and numbers of chromatin-bound molecules for each endogenous protein (Figure 4D). This analysis revealed that although the estimated concentrations of the different proteins were different by up to 3.75-fold (between 40 and 150 nM), the calculated numbers of chromatin-bound molecules were nevertheless remarkably similar at between 1700 and 4000. Taken together, these results demonstrate that independent calibration techniques give reliable measurement of molecule numbers, revealing highly consistent chromatin-bound quantities of the different proteins, despite their different kinetic characteristics.

ASH1 and PHO bind mitotic chromatin in neuroblasts

The live imaging analysis presented earlier in the text shows that the EGFP::ASH1 protein binds mitotic chromatin in embryos (Figure 2), and kinetic analysis defines quantitative parameters for chromatin binding in interphase (Figure 3). However, because of rapid chromatin movements and the short time of mitosis in preblastoderm embryos, it was not possible to perform kinetic analysis of metaphase chromatin. We have previously shown that larval NB and pupal SOP lineages are amenable to FRAP analysis in metaphase (17), identifying bound molecules that are not readily detectable by image analysis alone. This study reported the surprising finding that a small population of PC::EGFP molecules binds to both NB and SOP chromatin in metaphase with 10- and 300-fold longer residence times, respectively, than in interphase.

To determine whether a fraction of the PHO and E(Z) fusion proteins do indeed bind mitotic chromatin, and to study their kinetic behaviour, we performed live imaging and FRAP in type I NBs at interphase and metaphase (Figure 5, see also Figure 6A). Histone H2A fused to RFP (H2A::RFP) was used to mark chromatin and served as a guide for bleach spot placement on metaphase chromatin. The bound fraction of molecules was calculated as described earlier in the text for embryos, using the values of k^*_{on} and k_{off} extracted from FRAP data, [bound fraction = $k^*_{on}/(k^*_{on}+k_{off})$]. See Supplementary Table S1 for full listing of parameters and calculations. Analysis of metaphase FRAP data for EGFP::PHO revealed a bound fraction of ~1%, similar to that previously reported for PC::EGFP (Figure 5D and Supplementary Table S1). In contrast, no bound fraction

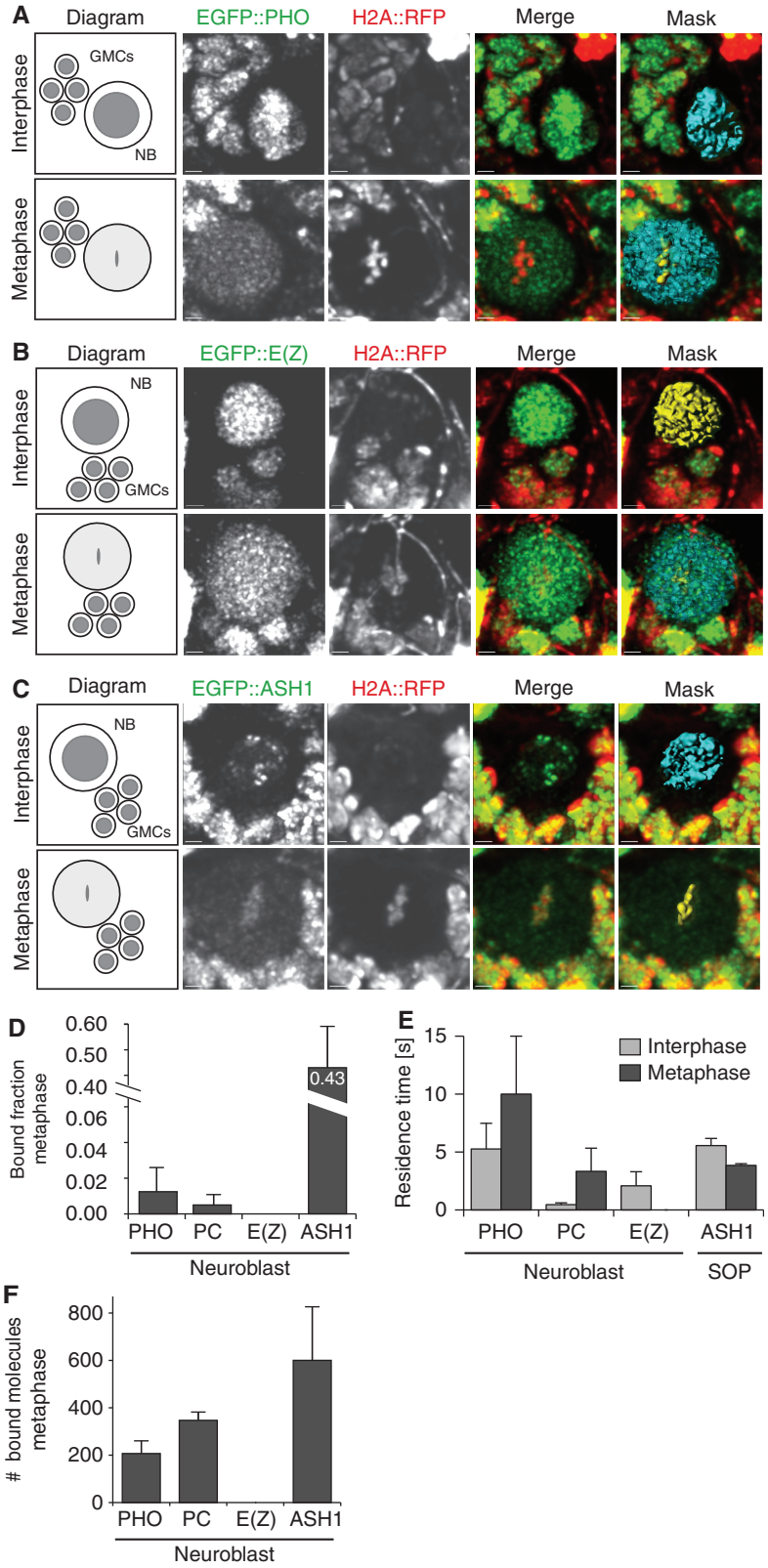

Figure 5. Quantification of chromatin binding in NB lineage. (**A–C**) Deconvolved confocal laser scanning images of EGFP::PHO (A), EGFP::E(Z) (B) and EGFP::ASH1 (C) in NB interphase (top row in each panel) and metaphase (bottom row in each panel). (Left) Diagrams identify NB and ganglion mother cells (GMCs) in images. H2A::RFP was used as a marker for chromatin. Merge panels show EGFP in green and H2A::RFP in red. Mask panels show the volumes occupied by EGFP in blue and the volume occupied by H2A::RFP in yellow. All EGFP:: fusion proteins shown were expressed under the *αTubulin* promoter. (**D**) Fraction of bound EGFP molecules calculated for PHO, PC and E(Z) using the values of k^*_{on} and k_{off} extracted from FRAP data [bound fraction = $k^*_{on}/(k^*_{on}+k_{off})$]. See Supplementary Table S1 for full listing of parameters and calculations. For ASH1, bound fraction was calculated by image analysis, see Supplementary Table S1. (**E**) Residence times measured by FRAP for EGFP::PHO,

(continued)

was detected for EGFP::E(Z), suggesting complete displacement from metaphase chromatin (Figure 5D and Supplementary Table S1). The low level of EGFP::ASH1 expression in NBs did not allow FRAP analysis in these cells. However, analysis of images showed that similarly to embryos, ASH1 was robustly detectable on metaphase chromatin in the NB lineage, representing 43% of the total protein. (Figure 5C and D and Supplementary Table S1).

To determine whether metaphase chromatin binding for EGFP::PHO and EGFP::ASH1 undergoes changes in kinetic properties, we examined residence times in interphase and metaphase. As aforementioned, because of the low level of EGFP::ASH1 in interphase (Figure 5C), it was not possible to perform FRAP on EGFP::ASH1 in NBs. However, kinetic parameters were extracted from FRAP performed in the SOP lineage, in which EGFP::ASH1 also visibly bound mitotic chromatin (Supplementary Figure S10). Neither EGFP::ASH1 nor EGFP::PHO protein showed a significant difference in residence time between interphase and metaphase (Figure 5E), thus the 10-fold increase observed for PC::EGFP seems to be unique for this protein (17). However, the mitotic residence times of both PHO and ASH1 were longer than for PC, indicating that each protein has specific and distinct behaviour.

To calculate the number of endogenous chromatin-bound molecules for each protein in metaphase, we performed VLP-mediated EGFP calibration and quantitative western blotting (Supplementary Figure S3). This analysis indicated that ~600 endogenous ASH1 molecules were bound to metaphase chromatin in NBs, in contrast to 207 for PHO and 347 for PC (17). In SOPs, in which EGFP::ASH1 is more highly expressed, we estimated the number of chromatin-bound ASH1 molecules at ~4000 (Supplementary Table S1), whereas PHO and E(Z) showed essentially identical behaviour as in NBs (data not shown). In summary, this analysis demonstrates that both EGFP::ASH1 and EGFP::PHO bind to mitotic chromatin in the NB lineage, and it indicates that substantially more ASH1 molecules remain bound than PHO or PC.

ASH1 and PC switch from an antagonistic to a cooperative relationship during mitosis

We have previously shown that the majority of PC::EGFP dissociates from NB chromatin at the onset of mitosis. Those molecules that do remain bound show 10-fold increase in their residence time (17). Here, we have shown that EGFP::ASH1 binds robustly to mitotic chromatin. PC and ASH1 share many chromatin targets (4), raising the possibility that they may bind mitotic chromatin by related mechanisms. To gain insight into the relationship between PC and ASH1 in interphase and mitosis, we performed RNAi-mediated knockdown of *ash1* in NBs and analysed the kinetic behaviour of PC::EGFP (Figure 6). *PcG* genes have been shown to be essential for NB survival (44). To determine whether *ash1* is also required for NB integrity, we asked whether *ash1* knockdown affects NB survival. *ash1* RNAi using the *inscuteable* GAL4 driver, which is expressed in all NBs (45), was lethal. In contrast, limiting *ash1* knockdown to only the type II NB lineage (Figure 6A and Supplementary Methods) gave viable flies, enabling examination of NB lineages in third instar larval brains. This analysis showed that the depletion of *ash1* led to a pronounced loss of NBs from the type II lineage, demonstrating that, like *PcG* genes, *ash1* is required for NB survival (Figure 6B and C). As RNAi was performed only in specific cell lineages, it was not possible to evaluate the knockdown efficiency in these cells. Instead, the efficiency of *ash1* knockdown was evaluated in late embryos using the ubiquitous *Actin5C* GAL4 driver, showing ~7-fold reduction of *ash1* transcript levels on RNAi knockdown (Figure 6D).

To investigate the effects of *ash1* knockdown on PC:EGFP kinetics, it was necessary to use transient RNAi expression to enable NB survival. For genetic reasons, it was not possible to achieve this specifically in the type II lineage (see Supplementary Methods). Instead, we performed *ash1* RNAi over a limited time window in all third instar larval NBs by transient induction of RNAi using the *inscuteable* GAL4 driver (see Supplementary Methods). Imaging and FRAP analysis was performed in type I NBs (Figure 6A), allowing comparison with previous results obtained from the same cell type [(17); Figure 5].

Analysis of fluorescence intensity showed that PC::EGFP protein levels themselves were unaffected by *ash1* knockdown (Figure 6E and F). PC::EGFP kinetics were analysed by FRAP. Calculation of the fraction of bound PC::EGFP molecules showed only modest changes in interphase and metaphase on *ash1* knockdown (Figure 6G and H; see also Supplementary Table S2). Surprisingly, *ash1* knockdown had opposite effects on PC::EGFP residence times in interphase and mitosis. In interphase, depletion of *ash1* led to a 2.5-fold increase in PC::EGFP residence time, consistent with an antagonistic relationship between the two proteins (Figure 6I). In contrast, in metaphase, *ash1* depletion resulted in a substantial decrease of PC::EGFP residence time, of ~3.7-fold (Figure 6J).

This change in residence time reflects a change in the parameter k_{off} ($T_{res} = 1/k_{off}$), whereas the absence of substantial change in bound molecule numbers reflects the fact that both k^*_{on} and k_{off} change in the knockdown [Bound fraction = $k^*_{on}/(k^*_{on} + k_{off})$]. The full set of kinetic parameters and calculations is given in Supplementary Table S2. As both the PC::EGFP protein levels and the numbers of bound molecules were largely

Figure 5. Continued
PC::EGFP, EGFP::E(Z) in NBs and EGFP::ASH1 in SOPs (Supplementary Figure S10) in interphase (light grey) and metaphase (dark grey). See also Supplementary Table S1. (**F**) Estimated number of endogenous molecules in wild-type NBs that are bound to metaphase chromatin. EGFP was quantified by VLP calibration. Endogenous molecule numbers were calculated on the basis of bound fractions shown in (D) and quantitative western blots shown in Supplementary Figure S3. See also Supplementary Table S1. All data show the mean and 95% confidence intervals of at least four cells.

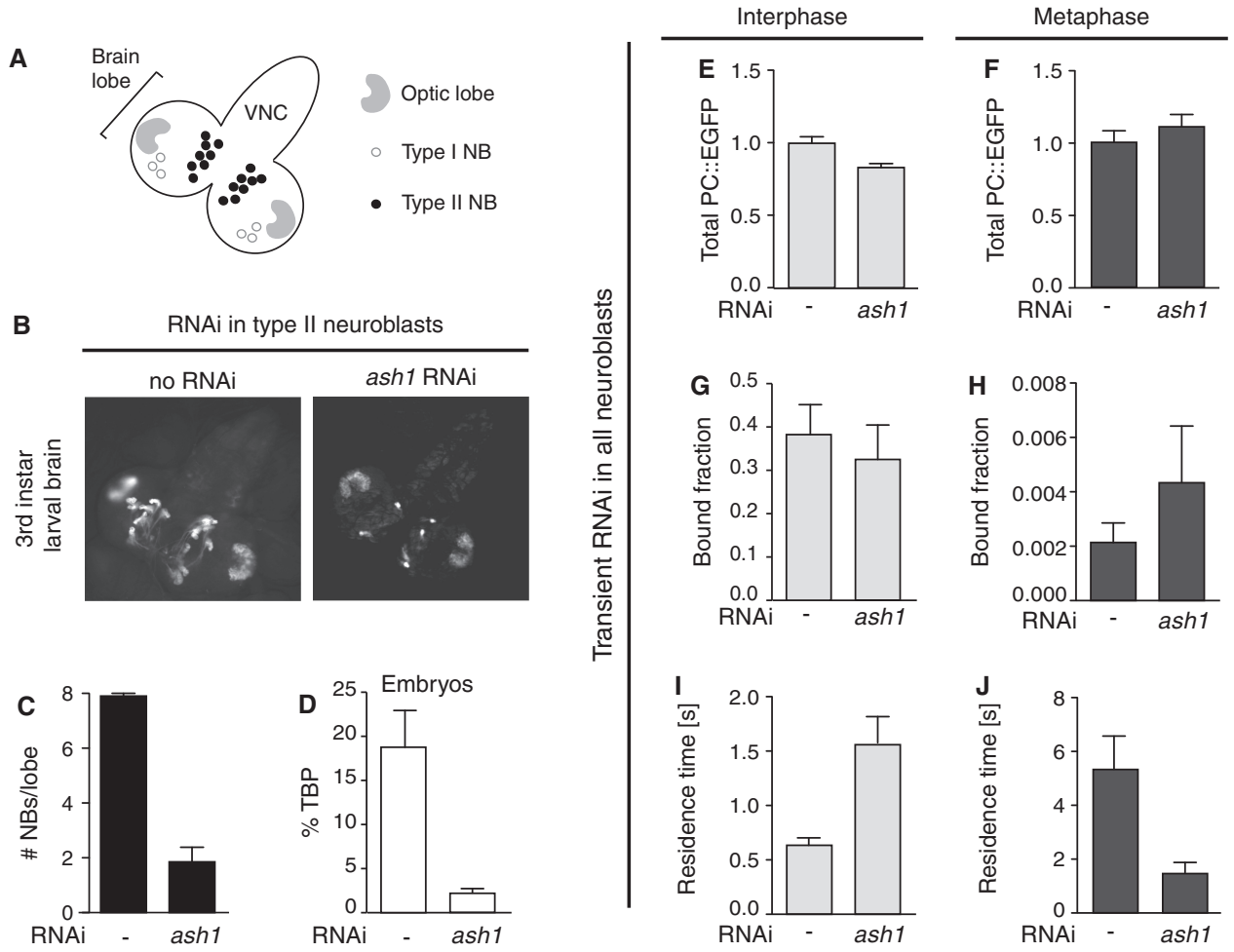

Figure 6. *ash1* knockdown modulates PC kinetics. (**A**) Diagram of third instar larval brain showing brain lobes and ventral nerve cord (VNC). The brain contains several classes of NBs (58). Those relevant to this study are the central brain NBs of type I (open circles) and type II (black circles). Only the NBs and not their daughter cells are shown in the diagram. Each brain lobe contains ~90 type I NBs and 8 type II NBs. (**B**) Images of third instar larval brains are shown in the same orientation as in (A). A GAL4 driver specific for type II NBs (see Supplementary Methods) was used to express either Upstream activating sequence-Green fluorescent protein (UAS-GFP) (left) or UAS-GFP together with a UAS-siRNA hairpin against *ash1* (59) (right) in type II NBs. In brains expressing *ash1* RNAi, the number of type II NBs was typically reduced to two to three per lobe. (**C**) Quantification of number of type II NBs per lobe from brain images represented in (B) showing mean and standard error from at least three brains. (**D**) siRNA-mediated knockdown of the *ash1* transcript was evaluated by RT–qPCR in embryos expressing either (left) an *Actin5C* GAL4 driver alone or (right) the same driver in combination with the UAS-*ash1* siRNA construct (see Supplementary Methods). *ash1* transcript levels are shown as percentage of the TBP transcript (TATA-binding protein). Data show mean and standard deviation of two independent experiments. (**E–J**) To overcome the cell lethality of *ash1* RNAi, transient expression of the UAS-*ash1* RNAi construct (59) was achieved using an *inscuteable*-GAL4 driver line, which is expressed in all NBs (45) in combination with GAL80ts (see Supplementary Methods) to achieve transient expression of the RNAi construct in NBs at third instar larval stages. These flies also carried the PC::EGFP transgene, enabling analysis of PC::EGFP kinetics. This analysis was performed in type I NBs [see (A)]. All data shown in (E–J) show mean and SEM of at least three experiments. (E,F) Quantification of GFP sum intensity in PC::EGFP expressing NBs in interphase (E) and metaphase (F) on expression of the driver alone, (left) or in combination with RNAi against *ash1* (right) showing no significant change in PC::EGFP molecule numbers on *ash1* knockdown. (G,H) Fraction of total PC::EGFP bound to chromatin in NB interphase (G) and metaphase (H) on no RNAi (left) or RNAi-mediated knockdown of *ash1* (right). Bound fractions were calculated from k^*_{on} and k_{off} values extracted from FRAP analysis (see legend to Supplementary Table S1 for calculations and Supplementary Table S2 for full listing of kinetic parameters). (I,J) Residence time of PC::EGFP in NB interphase (I) and metaphase (J) on no RNAi (left) or RNAi-mediated knockdown of *ash1* (right). Residence times were calculated from k_{off} extracted from FRAP analysis (see Supplementary Methods).

unaffected by *ash1* knockdown (Figure 6E–H), we reason that the differences in residence time reflect inherent properties of the PC::EGFP–chromatin interaction.

In summary, these results demonstrate that *ash1* is required for the increase in residence time of PC::EGFP on chromatin on the interphase to metaphase transition and suggest that the two proteins may switch from an antagonistic to a cooperative relationship during mitosis.

DISCUSSION

We have performed a quantitative live imaging analysis of the *Drosophila* PRC2 protein E(Z), the DNA-binding protein PHO and the TrxG protein ASH1, and compared their properties with those previously described for the PRC1 protein PC. By comparing key components involved in recruitment, activation and silencing, this study gives quantitative insights into dynamic aspects of

PcG and TrxG regulation and the molecular nature of mitotic memory.

In the course of this study, we generated and characterized three novel transgenic PcG and TrxG fusion proteins. All three can substitute for the *in vivo* function of their endogenous counterparts, are expressed at moderate levels in transgenic animals and give sufficient signal for imaging in living tissues; thus, these transgenes widen the repertoire of tools available for live imaging of PcG and TrxG proteins, which has previously been limited to PC (25) and PH (15). The expression levels of the fusion proteins are in the range of 1- to 5-fold compared with those of their endogenous counterparts. These levels of overexpression do not interfere with the physiological function of the proteins, and we did not observe any aberrant phenotypes in flies expressing the fusion proteins. In contrast, although heterozygous mutants in *PcG* and *trxG* genes are viable, they do show homeotic phenotypes (46). Together these observations suggest that the PcG and TrxG system is more sensitive to a reduction in protein levels than to an increase. However, there may be effects of the additional protein copies that are not readily detectable in terms of viability or phenotype.

Using these novel fusion proteins, we show that all of the proteins studied show highly dynamic chromatin binding, exchanging within seconds. We show that analysis of kinetics by FRAP and FCS shows excellent agreement in terms of the relative differences between proteins (Supplementary Figure S7E and F), which are the quantities of interest here. Chromatin-binding kinetics determined with fusion proteins expressed at different levels or in a mutant background (Supplementary Figure S5G, I, M and N) result in similar estimates, indicating that kinetic parameters are not influenced by the expression level of the fusion protein; thus, we reason that the kinetic measurements reported here are relevant to the wild-type situation in which lower levels of protein are present.

We have also performed absolute quantification of molecule numbers, giving estimates of cellular concentrations and chromatin-bound numbers in both interphase and mitosis, of both transgenic and endogenous molecules. Measurements of the numbers of EGFP fusion proteins showed excellent agreement between different techniques (Figure 4A). Estimations of endogenous molecule numbers, based on the ratio of fusion protein to endogenous protein determined from cell extracts, also showed good agreement between calculations based on different expression strategies (Figure 4B and C). Thus, we reason that we have obtained robust estimates for the total amount of endogenous protein per cell. This analysis revealed that the endogenous PcG and TrxG proteins are present in embryonic nuclei at between 40 and 150 nM (Figure 4D) and increase to between 200 and 400 nM in NBs (Supplementary Table S1). Knowledge of intracellular concentrations of these molecules is an essential step towards quantitative models of their function and places important constraints on the required affinity and abundance of binding sites for a productive interaction by mass action kinetics (18).

We used these measures of total molecule numbers in combination with bound fractions extracted from FRAP and FCS, to estimate numbers of endogenous chromatin-bound molecules (Figure 4D). These estimates have the limitation that they are based on the assumption that the bound fraction of fusion protein faithfully reflects the bound fraction of endogenous molecules. The fact that different expression levels of EGFP::ASH1 and EGFP::E(Z) did not significantly affect the bound fraction of transgenic molecules, (Supplementary Figures S5M and S6) suggests that this may indeed be the case for these proteins. However, as there is currently no method to directly test whether endogenous molecules are differently distributed between bound and free fractions than the GFP::fusion proteins, this remains a caveat. We note that potential uncertainty of the endogenous bound fraction will affect second order kinetic processes (on rates), but first order processes (off rates and, therefore, residence times) will be unaffected.

Despite these potential limitations, the comparison of different proteins yields valuable insights. For example, in early preblastoderm (2–3 h) embryos, we detected a robust fraction of chromatin-bound molecules for all four proteins (between 1700 and 4000 endogenous bound molecules, Figure 4D). This is consistent with ChIP-based observations of PcG and TrxG binding to Hox genes in the first 5 h of embryogenesis (47) and suggests early regulatory roles for the PcG and TrxG proteins. The residence times of all proteins were several seconds or less. This is comparable with residence times measured by similar methods for transcription factors and remodelers, but substantially shorter than those for promoter-bound and initiating polymerase II, [reviewed in (18)], raising questions about how the PcG and TrxG proteins interact in quantitative terms, in real-time, with the transcription machinery. Using the quantitative measurements of kinetic properties and molecular quantities presented here and elsewhere (18), it should be feasible in future to generate accurate mathematical models to address these issues.

The quantitative analysis presented here reveals not only similarities but also clear differences between the proteins that may be important for their distinct functions. For example, the DNA-binding protein PHO has up to 10-fold longer residence times than either PC or E(Z) in both embryos and NBs (Figure 3F and 5E). PHO has been shown to directly recruit complexes containing both E(Z) (35) and PC (34); thus, the longer residence time of PHO may reflect a more stable binding platform, which is 'visited' dynamically by the other PcG proteins. Like PC, the majority of chromatin-bound PHO molecules dissociate from mitotic chromatin, but several hundred molecules remain bound (Figures 5F and 7A). In contrast to PC, we did not observe a significant increase in the residence time of this bound population of PHO molecules. However, the mitotic residence time of PHO was still longer than for PC, again suggesting that PHO may provide a relatively stable binding platform for PC during mitosis, and that it may not change its mode of binding to chromatin on the interphase–metaphase transition. However, it will be important in future to determine whether PHO does indeed bind the same sites in

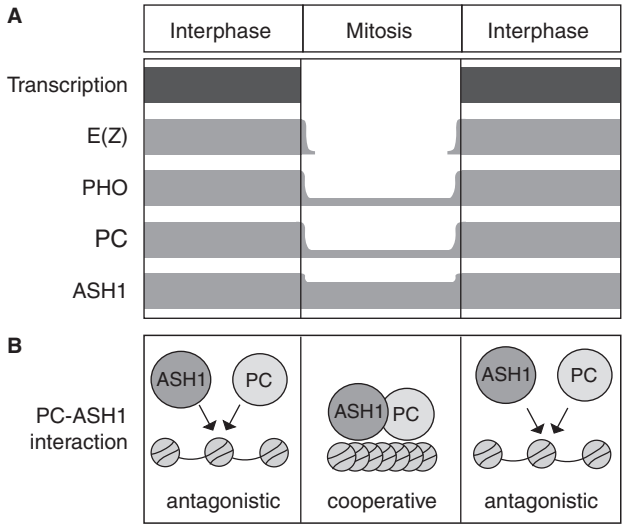

Figure 7. PcG and TrxG proteins bind differently to mitotic chromatin. (**A**) Summary of mitotic chromatin binding for E(Z), PHO and ASH1 (this study) and PC (17). Horizontal bars represent the extent of chromatin binding in interphase and metaphase (not drawn to scale). Top, dark grey bar: there is a global transcriptional shutdown in mitosis (54). E(Z) dissociates completely from mitotic chromatin. The majority (92–95%) of PC and PHO dissociates, but a few hundred molecules remain bound. In contrast, a large fraction of ASH1 remains bound to chromatin in mitosis. (**B**) *ash1* knockdown experiments indicate an antagonistic or competitive relationship between ASH1 and PC for chromatin binding in interphase, which switches to a cooperative one in metaphase. See 'Discussion' section for details.

interphase and mitosis, and whether it is required for anchoring PC to its binding sites during mitosis (34), or whether the increased residence time of PC reflects binding to chromatin via a different molecular interaction. Recent ChIP analysis of the PRC1 protein PSC shows that it binds to different sites on mitotic chromatin in interphase and mitosis (48). Similar analysis for PC and PHO may bring light to the interdependence of these proteins for mitotic binding. Surprisingly, RNAi knockdown of *pho* in NBs had no detectable effect on the kinetics of PC chromatin binding (data not shown); however, this may be due to the presence of PHO-like (PHOL), which functions redundantly with PHO (49). Concerted knockdown of *pho* and *phol* would be necessary to address whether these proteins have a role in mitotic anchoring of PC.

In contrast to PHO and PC, the E(Z) protein showed complete dissociation from mitotic chromatin (Figure 7A). Imaging of embryos (Figure 2C), SOPs (data not shown) and NBs (Figure 5B) showed no detectable bound protein. This result was confirmed by FRAP analysis of EGFP::E(Z) in metaphase NBs (Figure 5D). The complete dissociation of E(Z) from mitotic chromatin demonstrates that the physical presence of E(Z) is not required in mitosis for the binding of PC. It has been proposed that E(Z) is required for PC binding, by methylating lysine 27 of Histone H3 (H3K27me3), creating a binding platform for the PC chromodomain [for review see (37)]. It is possible that the E(Z)-independent binding of PC that we observe in metaphase is mediated by anchorage to H3K27me3 tails that persist through mitosis. However, we have recently shown that in both NBs and SOPs, there is a robust accumulation of H3S28 phosphorylation adjacent to sites of H3K27me3 at the onset of mitosis, which would preclude PC binding to H3K27me3 (17). This, in combination with the increased residence time of PC in mitosis, suggests that mitotic binding of PC is E(Z) and H3K27me3 independent, consistent with several reports of alternative mechanisms of PC binding to chromatin *in vitro* and at other cell cycle stages (20,22,23,34).

Surprisingly, the TrxG protein ASH1 showed the longest residence time of all proteins measured (Figure 3F and Supplementary Figures S5N and S7E). ASH1 has been shown genetically to act as an 'anti-repressor' to PcG action (6). Our results suggest that ASH1 may fulfil its functions not only by modifying the chromatin template (38) but also by its physical presence on chromatin. The behaviour of ASH1 in mitosis was strikingly different to that of the other proteins. In all cell types studied, EGFP::ASH1 was robustly and visibly bound to mitotic chromatin (Figures 2D, 5C and 7A and Supplementary Figure S10). Quantification by FRAP, FCS and direct image analysis indicates that although 51–62% of EGFP::ASH1 molecules are bound in interphase, between 36 and 51% of total molecules remain bound in metaphase (Supplementary Table S1). Indeed, we estimate that the fraction of bound ASH1 is reduced by no more than ~30% in any cell type, in strong contrast to the reduction in bound fraction of 92–100% observed for PHO, PC and E(Z) (Supplementary Table S1). The lower bound fraction of PcG proteins during mitosis suggests a role of mitotic chromatin retention of ASH1 for maintenance of active gene expression states. Such a role is consistent with models in which silencing is the default state (14), and genes that need to be reactivated are 'bookmarked'. The human TrxG protein MLL has been shown to bind mitotic chromatin in HeLa cells, whereas the ASH1 protein is evicted (27). The authors propose that mitotic bookmarking by MLL may facilitate inheritance of active gene expression states during cell division. Our results suggest that ASH1 may play an analogous role in *Drosophila*. Because of the complexity of TRX regulation, we were not able to address the TRX protein by live imaging. The transcript is alternatively spliced, and the protein itself is cleaved to N- and C-terminal parts, which have different, although incompletely characterized roles in gene regulation (4). However, TRX was detectable on mitotic chromatin by immunofluorescence staining; thus, in *Drosophila*, ASH1 and TRX may both be required for the mitotic memory of active states.

The fact that both PcG and TrxG proteins remain bound to mitotic chromatin, albeit to different extents (Figure 7A), is intriguing in light of a recent study reporting that both PcG and TrxG proteins, but not modified histones, remain associated with newly replicated chromatin in *Drosophila* embryos (22). Furthermore, the PRC1 protein PSC has recently been shown to be lost from PcG targets during mitosis but to be retained on a subset of sites that the authors propose may be important for

re-establishment of binding sites after mitosis (48). In light of these and our own findings, we propose that the 'default silencing' model may be an oversimplification, and that both TrxG and PcG proteins may be retained at specific sites both during replication and mitosis. It will be essential in future to determine whether these targets are different in different cell types.

By taking advantage of the genetic tools available in *Drosophila*, we have addressed interactions between different proteins, using cell-type–specific RNAi of one protein in combination with kinetic analysis of another. Surprisingly, knockdown of *ash1* in NBs had opposite effects on PC chromatin-binding kinetics in interphase and in metaphase, consistent with a switch in the functional relationship between ASH1 and PC during mitosis. These effects may be indirect, caused by loss of activation of ASH1 targets that are required to regulate PC binding. However, as ASH1 and PC share many chromatin targets (4), it is also likely that the effects of *ash1* knockdown on PC kinetics involve direct molecular interactions between the two proteins and the chromatin template (Figure 7B).

In interphase, depletion of *ash1* led to an increase in PC residence time on chromatin, suggesting an antagonistic relationship between the two proteins, consistent with genetic studies (6). The two proteins may compete directly for the same binding sites, for example, by competition for access to histones, to DNA or to DNA-binding proteins (Figure 7B). Interestingly, PHO has been shown to bind through different domains both to PC and to the BRM (Brahma) remodelling complex (34). It would be of great interest in future to determine whether PHO also binds ASH1. Alternatively, ASH1 may antagonize PC binding by modifying the chromatin template. ASH1 methylates Histone H3 on lysine 36 (38), which has been shown to antagonize PRC2-mediated H3K27 methylation (39). Thus, loss of ASH1 may lead to an increase in H3K27 methylation, which could lead to an increase in global PC-binding stability, reflected in a longer residence time.

The antagonistic relationship between ASH1 and PC that we observe for interphase chromatin binding is not surprising, given their opposite roles in activation and silencing. In contrast, for mitotic chromatin binding, *ash1* knockdown led to a decrease in PC residence time, indicating that the relationship between the two proteins switches from antagonistic to cooperative during mitosis (Figure 7B). Thus, the time for which PC is retained on mitotic chromatin depends on ASH1. This dependence may reflect a direct interaction between ASH1 and PC, for example, mediated by post-translational modifications of one or both proteins at mitosis, such that their affinity for each other increases (50). Alternatively, we envisage that the robust binding of ASH1 to mitotic chromatin may modify the template in such a way that binding sites for PC become available. In addition to histone templates, these sites may also include single-stranded DNA and non-coding RNAs [reviewed in (14)]. Finally, several histone-modifying enzymes have been shown to have additional non-histone targets (51,52), and ASH1 may be no exception. Thus, ASH1 may modify PC itself, in a cell cycle-specific manner, thereby altering its chromatin-binding properties. The molecular mechanisms by which ASH1 interacts with mitotic chromatin and influences PC will be key questions for future studies.

In summary, these findings suggest that mitotic memory of transcriptional states may involve active cooperation between PcG and TrxG proteins throughout the critical time window of mitosis. Why might such cooperativity be required? Correct maintenance of transcriptional states in interphase requires the dynamic and antagonistic interaction of both the PcG and TrxG proteins, ensuring flexibility of the system (53). However, during mitosis, transcriptional activity is globally shut down (54) (Figure 7A); thus, the PcG and TrxG are no longer required for transcriptional regulation. We envisage that it may be essential to maintain both the PcG and TrxG proteins on their chromatin target sites during mitosis to ensure their concerted presence at the next interphase. The requirement for both to be present may be met by co-operative binding to mitotic chromatin.

SUPPLEMENTARY DATA

Supplementary Data are available at NAR Online: Supplementary Tables 1 and 2, Supplementary Figures 1–10, Supplementary Methods and Supplementary References [55–64].

ACKNOWLEDGEMENTS

The authors are grateful to P. Pasierbek of the IMP/IMBA biooptics facility for advice and assistance on live imaging. They thank F. Müller for MATLAB files and advice on FRAP, D. Mazza for MATLAB files and advice on FCS and D. Poncet and A. Charpilienne for providing virus-like particles. They thank J. Knoblich, R. Paro, D. Arndt - Jovin and B. Dickson for fly stocks and R. Jones, J. Müller and F. Sauer for antibodies and cDNA constructs. They are grateful to C. Ehrhardt and C. Altmutter for technical assistance and D. Arndt - Jovin for helpful discussions.

FUNDING

Austrian Academy of Sciences http://www.oeaw.ac.at/ (to L.R., C.G. and E.D); EU FP6 Network of Excellence 'The Epigenome' http://www.epigenome-noe.net/ (to P.S.); EU FP7 Network of Excellence 'Epigenesys' http://www.epigenesys.eu/ (to P.S.); Portuguese Foundation for Science and Technology http://www.fct.pt/ (SFRH/BD/40389/2007) (to J.P.F.). The funders had no role in study design, data collection and analysis, decision to publish, or preparation of the manuscript. Funding for open access charge: Austrian Academy of Sciences.

Conflict of interest statement. None declared.

REFERENCES

1. Schwartz,Y.B. and Pirrotta,V. (2007) Polycomb silencing mechanisms and the management of genomic programmes. *Nat. Rev. Genet.*, **8**, 9–22.
2. Schuettengruber,B., Martinez,A.M., Iovino,N. and Cavalli,G. (2011) Trithorax group proteins: switching genes on and keeping them active. *Nat. Rev. Mol. Cell Biol.*, **12**, 799–814.
3. Schuettengruber,B., Ganapathi,M., Leblanc,B., Portoso,M., Jaschek,R., Tolhuis,B., van Lohuizen,M., Tanay,A. and Cavalli,G. (2009) Functional anatomy of polycomb and trithorax chromatin landscapes in *Drosophila* embryos. *PLoS Biol.*, **7**, e13.
4. Schwartz,Y.B., Kahn,T.G., Stenberg,P., Ohno,K., Bourgon,R. and Pirrotta,V. (2010) Alternative epigenetic chromatin states of polycomb target genes. *PLoS Genet.*, **6**, e1000805.
5. Enderle,D., Beisel,C., Stadler,M.B., Gerstung,M., Athri,P. and Paro,R. (2011) Polycomb preferentially targets stalled promoters of coding and noncoding transcripts. *Genome Res.*, **21**, 216–226.
6. Klymenko,T. and Muller,J. (2004) The histone methyltransferases Trithorax and Ash1 prevent transcriptional silencing by Polycomb group proteins. *EMBO Rep.*, **5**, 373–377.
7. Simon,J., Chiang,A., Bender,W., Shimell,M.J. and O'Connor,M. (1993) Elements of the *Drosophila* bithorax complex that mediate repression by Polycomb group products. *Dev. Biol.*, **158**, 131–144.
8. Chan,C.S., Rastelli,L. and Pirrotta,V. (1994) A Polycomb response element in the Ubx gene that determines an epigenetically inherited state of repression. *EMBO J.*, **13**, 2553–2564.
9. Cavalli,G. and Paro,R. (1998) The *Drosophila* Fab-7 chromosomal element conveys epigenetic inheritance during mitosis and meiosis. *Cell*, **93**, 505–518.
10. Maurange,C. and Paro,R. (2002) A cellular memory module conveys epigenetic inheritance of hedgehog expression during *Drosophila* wing imaginal disc development. *Genes Dev.*, **16**, 2672–2683.
11. Perez,L., Barrio,L., Cano,D., Fiuza,U.M., Muzzopappa,M. and Milan,M. (2011) Enhancer-PRE communication contributes to the expansion of gene expression domains in proliferating primordia. *Development*, **138**, 3125–3134.
12. Mohn,F., Weber,M., Rebhan,M., Roloff,T.C., Richter,J., Stadler,M.B., Bibel,M. and Schubeler,D. (2008) Lineage-specific polycomb targets and de novo DNA methylation define restriction and potential of neuronal progenitors. *Mol. Cell*, **30**, 755–766.
13. Muller,J. and Kassis,J.A. (2006) Polycomb response elements and targeting of Polycomb group proteins in *Drosophila*. *Curr. Opin. Genet. Dev.*, **16**, 476–484.
14. Ringrose,L. and Paro,R. (2007) Polycomb/Trithorax response elements and epigenetic memory of cell identity. *Development*, **134**, 223–232.
15. Ficz,G., Heintzmann,R. and Arndt-Jovin,D.J. (2005) Polycomb group protein complexes exchange rapidly in living *Drosophila*. *Development*, **132**, 3963–3976.
16. Ren,X., Vincenz,C. and Kerppola,T.K. (2008) Changes in the distributions and dynamics of polycomb repressive complexes during embryonic stem cell differentiation. *Mol. Cell Biol.*, **28**, 2884–2895.
17. Fonseca,J.P., Steffen,P.A., Muller,S., Lu,J., Sawicka,A., Seiser,C. and Ringrose,L. (2012) *In vivo* Polycomb kinetics and mitotic chromatin binding distinguish stem cells from differentiated cells. *Genes Dev.*, **26**, 857–871.
18. Steffen,P.A., Fonseca,J.P. and Ringrose,L. (2012) Epigenetics meets mathematics: towards a quantitative understanding of chromatin biology. *Bioessays*, **34**, 901–913.
19. Hansen,K.H., Bracken,A.P., Pasini,D., Dietrich,N., Gehani,S.S., Monrad,A., Rappsilber,J., Lerdrup,M. and Helin,K. (2008) A model for transmission of the H3K27me3 epigenetic mark. *Nat. Cell Biol.*, **10**, 1291–1300.
20. Francis,N.J., Follmer,N.E., Simon,M.D., Aghia,G. and Butler,J.D. (2009) Polycomb proteins remain bound to chromatin and DNA during DNA replication *in vitro*. *Cell*, **137**, 110–122.
21. Lanzuolo,C., Lo Sardo,F., Diamantini,A. and Orlando,V. (2011) PcG complexes set the stage for epigenetic inheritance of gene silencing in early S phase before replication. *PLoS Genet.*, **7**, e1002370.
22. Petruk,S., Sedkov,Y., Johnston,D.M., Hodgson,J.W., Black,K.L., Kovermann,S.K., Beck,S., Canaani,E., Brock,H.W. and Mazo,A. (2012) TrxG and PcG proteins but not methylated histones remain associated with DNA through replication. *Cell*, **150**, 922–933.
23. Lo,S.M., Follmer,N.E., Lengsfeld,B.M., Madamba,E.V., Seong,S., Grau,D.J. and Francis,N.J. (2012) A bridging model for persistence of a polycomb group protein complex through DNA replication *in vitro*. *Mol. Cell*, **46**, 784–796.
24. Buchenau,P., Hodgson,J., Strutt,H. and Arndt-Jovin,D.J. (1998) The distribution of polycomb-group proteins during cell division and development in *Drosophila* embryos: impact on models for silencing. *J. Cell. Biol.*, **141**, 469–481.
25. Dietzel,S., Niemann,H., Bruckner,B., Maurange,C. and Paro,R. (1999) The nuclear distribution of Polycomb during *Drosophila* melanogaster development shown with a GFP fusion protein. *Chromosoma*, **108**, 83–94.
26. Mishra,B.P., Ansari,K.I. and Mandal,S.S. (2009) Dynamic association of MLL1, H3K4 trimethylation with chromatin and Hox gene expression during the cell cycle. *FEBS J.*, **276**, 1629–1640.
27. Blobel,G.A., Kadauke,S., Wang,E., Lau,A.W., Zuber,J., Chou,M.M. and Vakoc,C.R. (2009) A reconfigured pattern of MLL occupancy within mitotic chromatin promotes rapid transcriptional reactivation following mitotic exit. *Mol. Cell*, **36**, 970–983.
28. Ringrose,L. (2009) Transgenesis in *Drosophila* melanogaster. *Methods Mol. Biol.*, **561**, 3–19.
29. Nedelec,F., Surrey,T. and Maggs,A.C. (2001) Dynamic concentration of motors in microtubule arrays. *Phys. Rev. Lett.*, **86**, 3192–3195.
30. Mueller,F., Wach,P. and McNally,J.G. (2008) Evidence for a common mode of transcription factor interaction with chromatin as revealed by improved quantitative fluorescence recovery after photobleaching. *Biophys. J.*, **94**, 3323–3339.
31. Michelman-Ribeiro,A., Mazza,D., Rosales,T., Stasevich,T.J., Boukari,H., Rishi,V., Vinson,C., Knutson,J.R. and McNally,J.G. (2009) Direct measurement of association and dissociation rates of DNA binding in live cells by fluorescence correlation spectroscopy. *Biophys. J.*, **97**, 337–346.
32. Culbertson,C.T., Jacobson,S.C. and Michael Ramsey,J. (2002) Diffusion coefficient measurements in microfluidic devices. *Talanta*, **56**, 365–373.
33. Brown,J.L., Mucci,D., Whiteley,M., Dirksen,M.L. and Kassis,J.A. (1998) The *Drosophila* Polycomb group gene pleiohomeotic encodes a DNA binding protein with homology to the transcription factor YY1. *Mol. Cell*, **1**, 1057–1064.
34. Mohd-Sarip,A., Venturini,F., Chalkley,G.E. and Verrijzer,C.P. (2002) Pleiohomeotic can link polycomb to DNA and mediate transcriptional repression. *Mol. Cell Biol.*, **22**, 7473–7483.
35. Wang,L., Brown,J.L., Cao,R., Zhang,Y., Kassis,J.A. and Jones,R.S. (2004) Hierarchical recruitment of polycomb group silencing complexes. *Mol. Cell*, **14**, 637–646.
36. Klymenko,T., Papp,B., Fischle,W., Kocher,T., Schelder,M., Fritsch,C., Wild,B., Wilm,M. and Muller,J. (2006) A Polycomb group protein complex with sequence-specific DNA-binding and selective methyl-lysine-binding activities. *Genes Dev.*, **20**, 1110–1122.
37. Margueron,R. and Reinberg,D. (2011) The Polycomb complex PRC2 and its mark in life. *Nature*, **469**, 343–349.
38. Tanaka,Y., Katagiri,Z., Kawahashi,K., Kioussis,D. and Kitajima,S. (2007) Trithorax-group protein ASH1 methylates histone H3 lysine 36. *Gene*, **397**, 161–168.
39. Yuan,W., Xu,M., Huang,C., Liu,N., Chen,S. and Zhu,B. (2011) H3K36 methylation antagonizes PRC2-mediated H3K27 methylation. *J. Biol. Chem.*, **286**, 7983–7989.
40. Groth,A.C., Fish,M., Nusse,R. and Calos,M.P. (2004) Construction of transgenic *Drosophila* by using the site-specific integrase from phage phiC31. *Genetics*, **166**, 1775–1782.
41. Foe,V.E. and Alberts,B.M. (1983) Studies of nuclear and cytoplasmic behaviour during the five mitotic cycles that precede gastrulation in *Drosophila* embryogenesis. *J. Cell Sci.*, **61**, 31–70.

42. Stasevich,T.J., Mueller,F., Michelman-Ribeiro,A., Rosales,T., Knutson,J.R. and McNally,J.G. (2010) Cross-validating FRAP and FCS to quantify the impact of photobleaching on *in vivo* binding estimates. *Biophys. J.*, **99**, 3093–3101.
43. Dundr,M., McNally,J.G., Cohen,J. and Misteli,T. (2002) Quantitation of GFP-fusion proteins in single living cells. *J. Struct. Biol.*, **140**, 92–99.
44. Bello,B., Holbro,N. and Reichert,H. (2007) Polycomb group genes are required for neural stem cell survival in postembryonic neurogenesis of *Drosophila*. *Development*, **134**, 1091–1099.
45. Kraut,R. and Campos-Ortega,J.A. (1996) inscuteable, a neural precursor gene of *Drosophila*, encodes a candidate for a cytoskeleton adaptor protein. *Dev. Biol.*, **174**, 65–81.
46. Kennison,J.A. (1995) The Polycomb and trithorax group proteins of *Drosophila*: trans-regulators of homeotic gene function. *Annu. Rev. Genet.*, **29**, 289–303.
47. Orlando,V., Jane,E.P., Chinwalla,V., Harte,P.J. and Paro,R. (1998) Binding of trithorax and Polycomb proteins to the bithorax complex: dynamic changes during early *Drosophila* embryogenesis. *EMBO J.*, **17**, 5141–5150.
48. Follmer,N.E., Wani,A.H. and Francis,N.J. (2013) A polycomb group protein is retained at specific sites on chromatin in mitosis. *PLoS Genet.*, **8**, e1003135.
49. Brown,J.L., Fritsch,C., Mueller,J. and Kassis,J.A. (2003) The *Drosophila* pho-like gene encodes a YY1-related DNA binding protein that is redundant with pleiohomeotic in homeotic gene silencing. *Development*, **130**, 285–294.
50. Niessen,H.E., Demmers,J.A. and Voncken,J.W. (2009) Talking to chromatin: post-translational modulation of polycomb group function. *Epigenetics Chromatin*, **2**, 10.
51. Sampath,S.C., Marazzi,I., Yap,K.L., Krutchinsky,A.N., Mecklenbrauker,I., Viale,A., Rudensky,E., Zhou,M.M., Chait,B.T. and Tarakhovsky,A. (2007) Methylation of a histone mimic within the histone methyltransferase G9a regulates protein complex assembly. *Mol. Cell*, **27**, 596–608.
52. Mohd-Sarip,A., Lagarou,A., Doyen,C.M., van der Knaap,J.A., Aslan,U., Bezstarosti,K., Yassin,Y., Brock,H.W., Demmers,J.A. and Verrijzer,C.P. (2012) Transcription-independent function of Polycomb group protein PSC in cell cycle control. *Science*, **336**, 744–747.
53. Ringrose,L. and Paro,R. (2004) Epigenetic regulation of cellular memory by the Polycomb and Trithorax group proteins. *Annu. Rev. Genet.*, **38**, 413–443.
54. Gottesfeld,J.M. and Forbes,D.J. (1997) Mitotic repression of the transcriptional machinery. *Trends Biochem. Sci.*, **22**, 197–202.
55. Carrington,E.A. and Jones,R.S. (1996) The *Drosophila* enhancer of zeste gene encodes a chromosomal protein: examination of wild-type and mutant protein distribution. *Development*, **122**, 4073–4083.
56. Tripoulas,N., LaJeunesse,D., Gildea,J. and Shearn,A. (1996) The *Drosophila* ash1 gene product, which is localized at specific sites on polytene chromosomes, contains a SET domain and a PHD finger. *Genetics*, **143**, 913–928.
57. Beisel,C., Imhof,A., Greene,J., Kremmer,E. and Sauer,F. (2002) Histone methylation by the *Drosophila* epigenetic transcriptional regulator Ash1. *Nature*, **419**, 857–862.
58. Homem,C.C. and Knoblich,J.A. (2012) *Drosophila* neuroblasts: a model for stem cell biology. *Development*, **139**, 4297–4310.
59. Dietzl,G., Chen,D., Schnorrer,F., Su,K.C., Barinova,Y., Fellner,M., Gasser,B., Kinsey,K., Oppel,S., Scheiblauer,S. *et al.* (2007) A genome-wide transgenic RNAi library for conditional gene inactivation in *Drosophila*. *Nature*, **448**, 151–156.
60. Okulski,H., Druck,B., Bhalerao,S. and Ringrose,L. (2011) Quantitative analysis of polycomb response elements (PREs) at identical genomic locations distinguishes contributions of PRE sequence and genomic environment. *Epigenetics Chromatin*, **4**, 4.
61. Müller,J., Hart,C., Francis,N., Vargas,M., Sengupta,A., Wild,B., Miller,E., O'Connor,M., Kingston,R. and Simon,J. (2002) Histone methyltransferase activity of a *Drosophila* Polycomb group repressor complex. *Cell*, **111**, 197–208.
62. Bayraktar,O.A., Boone,J.Q., Drummond,M.L. and Doe,C.Q. (2010) *Drosophila* type II neuroblast lineages keep Prospero levels low to generate large clones that contribute to the adult brain central complex. *Neural Dev.*, **5**, 26.
63. Papp,B. and Muller,J. (2006) Histone trimethylation and the maintenance of transcriptional ON and OFF states by trxG and PcG proteins. *Genes Dev.*, **20**, 2041–2054.
64. Beisel,C., Buness,A., Roustan-Espinosa,I.M., Koch,B., Schmitt,S., Haas,S.A., Hild,M., Katsuyama,T. and Paro,R. (2007) Comparing active and repressed expression states of genes controlled by the Polycomb/Trithorax group proteins. *Proc. Natl Acad. Sci. USA*, **104**, 16615–16620.